Investigation of Microstructure in Poly[(*p*-hydroxybenzoic acid)-*co*-(ethylene terephthalate)] Using Nuclear Magnetic Resonance Spectroscopy

Karl R. Amundson,*,† Jeffrey A. Reimer, and Morton M. Denn

Department of Chemical Engineering, University of California at Berkeley, and Center for Advanced Materials, Lawrence Berkeley Laboratory, Berkeley, California 94720

Received October 4, 1990; Revised Manuscript Received December 18, 1990

ABSTRACT: The microstructure and dynamics of liquid crystalline copolymers of *p*-hydroxybenzoic acid (HBA) and ethylene terephthalate (ETP) were investigated by proton and ^{13}C solid-state NMR spectroscopy. The HBA/ETP 80/20 (80 mol % HBA) copolymer contains poly(HBA)-like crystallites with a mass fraction of 4–7% and a smallest linear dimension of about 80 Å. The dominant crystal structures in HBA/ETP 60/40 (60 mol % HBA) have a similar mass fraction but resemble poly(ethylene terephthalate) crystallites. NMR spin-lock relaxation indicates cooperative motion in both copolymers above 130 °C involving small angular fluctuations of the local polymer chain axis about the local nematic director. A minority "rigid" component in HBA/ETP 80/20, which is 22–28% abundant at 150 °C and about 15% abundant at 290 °C, does not exhibit cooperative motion. HBA/ETP 60/40 displays similar behavior. Static ^{13}C NMR line shapes indicate that aromatic rings exhibit free rotation about the polymer chain axis within the component that exhibits cooperative motion, while aromatic rings exhibit small-angle ($\sim 20°$) fluctuations about their substituted axes in the rigid component. ^{13}C MAS NMR shows that the compositions of the rigid components in both copolymers above 130 °C are nearly the same as the bulk compositions. The observed behavior is consistent with the presence of nonperiodic layer crystallites.

Introduction

Random copolymers of *p*-hydroxybenzoic acid (HBA) and ethylene terephthalate (ETP) have received much attention because they exhibit a nematic liquid crystalline phase upon melting. The microstructuure of HBA/ETP copolymers has been studied extensively by calorimetry,[1] diffraction,[2-4] microscopy,[2,4] chemical etching,[5] dielectric spectroscopy,[6,7] and nuclear magnetic resonance (NMR) spectroscopy.[8-12] Although there is not complete agreement, the general consensus is that HBA/ETP copolymers exhibit a complex microstructure as evidenced by the presence of two glass transitions,[1] a spatially heterogeneous HBA monomer concentration,[2-5] and homopolymer-like crystallites.[2-4,13] It is likely that these microstructural features play a significant role in the complex melt rheological behavior of HBA/ETP copolymers, including viscosity power law behavior that persists over more than eight decades of shear rate and reversible transient growth of the storage modulus.[14] This paper presents an investigation into the microstructure of HBA/ETP copolymers by means of solid-state NMR spectroscopy. In particular, two issues are addressed: the nature of crystallites in HBA/ETP copolymers and the nature and spatial heterogeneity of molecular motion associated with the glass transitions. HBA/ETP 80/20 and HBA/ETP 60/40 (80 and 60 mol % HBA, respectively) were studied. The 80/20 composition is fully nematic in the melt, while the 60/40 composition contains isotropic material.[9,10,15] Proton spin-lock relaxation was used to characterize slow (mid-kilohertz frequency) molecular motion. Proton and ^{13}C spectra were used to determine chemical structure and molecular dynamics, and proton spin diffusion was used to measure microstructural geometry.

Experimental Section

Materials. HBA/ETP 80/20 and HBA/ETP 60/40 polymer samples were provided by Tennessee Eastman Co. in the form of extruded pellets and flakes. Polymer samples were dried under vacuum at 130 °C for approximately 2 days and then flame-sealed under vacuum in Pyrex NMR tubes. Most experiments were performed on polymer samples as received from Tennessee Eastman (extruded from the melt). Experiments were also performed on polymer samples that were heated to the melt (310 °C for HBA/ETP 80/20 and 250 °C for HBA/ETP 60/40) and then either slowly cooled (5 or 10 °C/min) on a Mettler FP82 programmable hot stage or quenched in liquid nitrogen. The melt temperatures were chosen to be well-above reported melt transitions.[1]

NMR Experiments. All NMR experiments, except ^{13}C magic angle spinning experiments, were performed on a home-built 180-MHz NMR spectrometer. Proton free induction decays (FIDs) were collected after a 1–2-μs excitation pulse. Presumably because of molecular motion, solid-echo experiments resulted in much line-shape distortion, and so FIDs were collected immediately after an excitation pulse and the initial FID data lost due to the 7–9-μs spectrometer recovery time were reconstructed by an extrapolation of a polynomial fit to the undistorted portion of the FID.[15] Spin-lock relaxation experiments were performed by application of a resonant spin-lock field (typically 5 or 10 G) phase shifted 90° from the excitation pulse. Relaxation of transverse magnetization was monitored by measuring the FID amplitude after various spin-lock times, and a weighted least-squares minimization routine was used to fit the spin–lock relaxation data to a single-exponential decay or sum of two exponential decays in order to determine $T_{1\rho}$ values. All spin-lock relaxation experiments performed with a 5-G field strength were repeated using a 10-G field strength as a precaution against anomalous behavior due to local dipolar field effects. The relaxation behavior at the two field strengths was always very similar. In addition, the proton line shape as a function of spin-lock time was monitored to ensure that the observed nonexponential relaxation behavior was not due to anisotropy in $T_{1\rho}$. In all cases, there was no significant change in the proton line shape with spin-lock time beyond some broadening, and this was caused by increased rigidity of the long-$T_{1\rho}$ component.

Spin-diffusion experiments involved three steps: preparation, diffusion, and detection. In the preparation step, transverse proton magnetization was created by a $\pi/2$ pulse and then spin-locked for 12 ms in order to eliminate the magnetization in the short-$T_{1\rho}$ component of the sample, after which the magnetization was rotated back to the magnetic field axis by another $\pi/2$ pulse.

* To whom correspondence should be addressed.
† Present address: AT&T Bell Laboratories, 600 Mountain Ave., Murray Hill, NJ 07974.

0024-9297/91/2224-3250$02.50/0

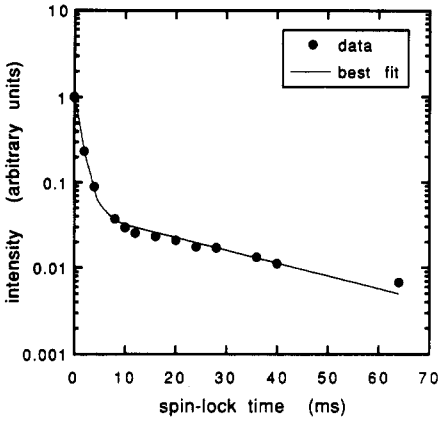

Figure 1. Free induction decay intensity as a function of the spin-lock time for HBA/ETP 80/20 at 24 °C. The solid line is a best fit of the data based upon a two-exponential decay.

The diffusion step was merely a delay of time τ_d in which spin energy was allowed to diffuse across spin energy gradients. Finally, in the detection step, magnetization was rotated back to the transverse plane, and the spin-lock relaxation behavior was measured by detection of the FID after several spin-lock times. Reemergence of a short-$T_{1\rho}$ signal indicated the occurrence of spin diffusion.

Nonspinning ^{13}C FID signals were collected after cross-polarization with protons for 2 ms. The Hartmann–Hahn frequency and proton-decouple frequency were 21 kHz. ^{13}C spectra of the long proton $T_{1\rho}$ components were collected by proton spin-lock relaxation followed by cross-polarization and detection of the ^{13}C signal; in each case the spin-lock relaxation time was chosen so that the short-$T_{1\rho}$ proton magnetization was insignificant at the end of the spin-lock.

A home-built heater surrounding the NMR probe sample solenoid was used for elevated-temperature studies. The heater element consisted of nichrome wire windings inside a layer of heat-treated Fiberfrax insulation. Care was taken to minimize the mutual inductance between the NMR solenoid and the nichrome wire windings. Design details can be found in ref 15. To avoid interference from the magnetic field emanating from the heater current, the heater current was interrupted during and 50-ms prior to pulse sequences and signal detection.

Room temperature ^{13}C cross-polarization (CP) magic angle spinning (MAS) NMR experiments were performed on the University of California College of Chemistry's home-built 180-MHz NMR spectrometer with a Nicolet data station. It was equipped with a Doty double-resonance MAS probe. The cross-polarization time was 1 ms, and the Hartmann–Hahn frequency and proton-decouple frequency were 40 kHz. Elevated-temperature ^{13}C CP MAS NMR was performed by Dr. Grant Haddix at Shell Development Corp., Westhollow Research Center using a 200-MHz spectrometer. ^{13}C spectra were collected after a 1–3-ms cross-polarization with protons. The Hartmann–Hahn and proton-decouple frequencies were 50 kHz. The proton spin-lock field strengths were adjusted to match those of prior proton spin-lock relaxation experiments. In this way, the results from the various spectrometers could be related.

Investigation of Crystallites. Experiments and Results

Proton Spin-Lock Relaxation and ^{13}C MAS NMR. The spin-lock relaxation behavior of protons in HBA/ETP 80/20 is described well by a sum of two exponential decays; the long-$T_{1\rho}$ component is typically between 4 and 7% (Figure 1 and Table I). The proton line shape of the long-$T_{1\rho}$ component is slightly broader than the line shape of the total polymer sample (Figure 2). With an increase in temperature from 24 to 125 °C, the line shape from the total polymer sample narrowed significantly so that a doublet character is apparent. The doublet character results from the strong dipolar couplings between neighboring protons on aromatic rings. At room temperature this doublet is broadened by intermolecular and other intramolecular dipolar couplings, while at 125 °C aromatic ring motion is sufficient to greatly reduce these couplings. The long-$T_{1\rho}$ line shape, on the other hand, still exhibits strong intermolecular couplings at 125 °C, and so this component is more rigid than the rest of the polymer. Figure 3 shows ^{13}C spectra of (a) the entire polymer sample and (b) the long proton $T_{1\rho}$ component. The similarity between the long-$T_{1\rho}$ spectrum and the spectrum of poly(HBA) (Figure 3c) indicates that the long-$T_{1\rho}$ component is rich in the HBA monomer. The sharp lines of the long-$T_{1\rho}$ spectrum are indicative of either regions of high molecular mobility or a more uniform environment than the surrounding liquid crystal glass environment, i.e., a crystalline phase. The broadness of the long-$T_{1\rho}$ proton line shapes indicates the latter. Therefore, the long-$T_{1\rho}$ component of HBA/ETP 80/20 is poly(HBA)-like crystallites.

Table I
Best-Fit Parameters for Spin-Lock Relaxation of Protons in HBA/ETP 80/20 and 60/40

	short $T_{1\rho}$, ms	long $T_{1\rho}$, ms	long-$T_{1\rho}$ fraction
HBA/ETP 80/20	1.4	33	5%[a]
HBA/ETP 60/40	1.6	15	5%[b]

[a] Typical value between 4 and 7%. [b] Typical value between 4 and 5%.

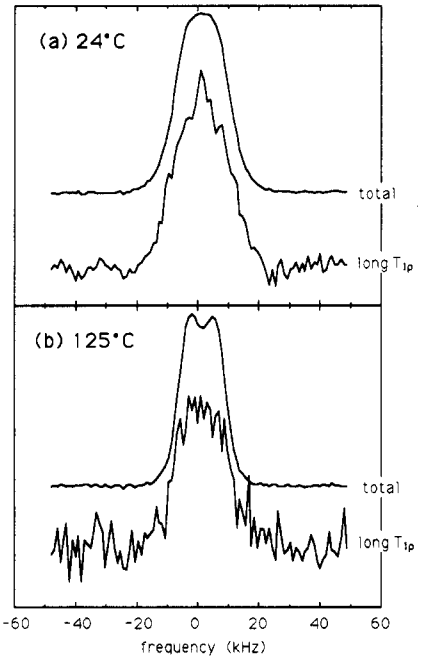

Figure 2. Total and long-$T_{1\rho}$ proton line shapes of HBA/ETP 80/20 at (a) 24 °C and (b) 125 °C. The long-$T_{1\rho}$ line shapes were collected after spin locking for sufficient time to suppress the short-$T_{1\rho}$ magnetization. The dipolar interaction between nearest-neighbor aromatic protons gives rise to the doublet character, which becomes clear at 125 °C where molecular motion reduces the intermolecular interactions. The small narrow peak in the long-$T_{1\rho}$ line shape at 24 °C is probable due to a mobile impurity such as residual water or monomer.

The spin-lock relaxation behavior of protons in HBA/ETP 60/40 was also described well by a sum of two exponential decays; best-fit parameters are shown in Table I. The proton line shapes were also very similar to the line shapes of HBA/ETP 80/20. The bulk and long proton $T_{1\rho}$ ^{13}C spectra of as-received HBA/ETP 60/40 are shown in Figure 4. The long proton $T_{1\rho}$ ^{13}C spectrum for this composition matches the ^{13}C spectrum of poly(ethylene terephthalate) (PET) shown in Figure 4c. The aliphatic carbon peak of PET can be divided into a sharp peak at

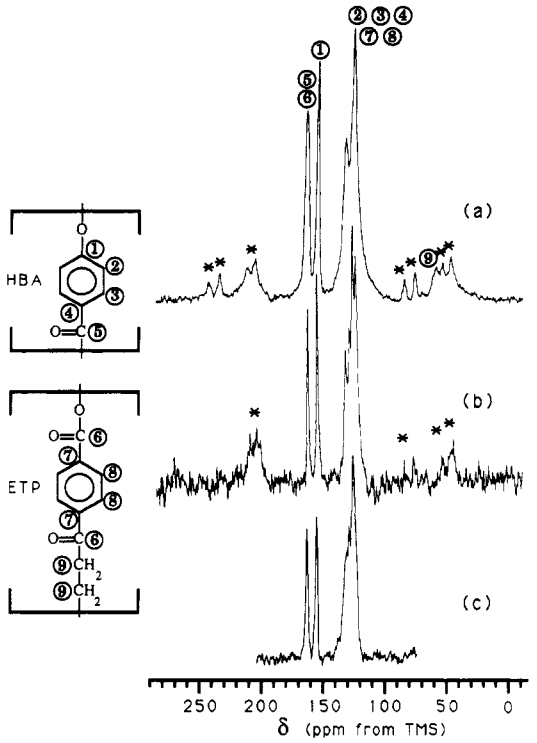

Figure 3. ^{13}C CP MAS spectra of (a) HBA/ETP 80/20, (b) the long-$T_{1\rho}$ component of HBA/PET 80/20, and (c) poly(HBA). The latter is taken from ref 25. Peak assignments are indicated by the circled numbers and the chart to the left. Asterisks indicate spinning sidebands.

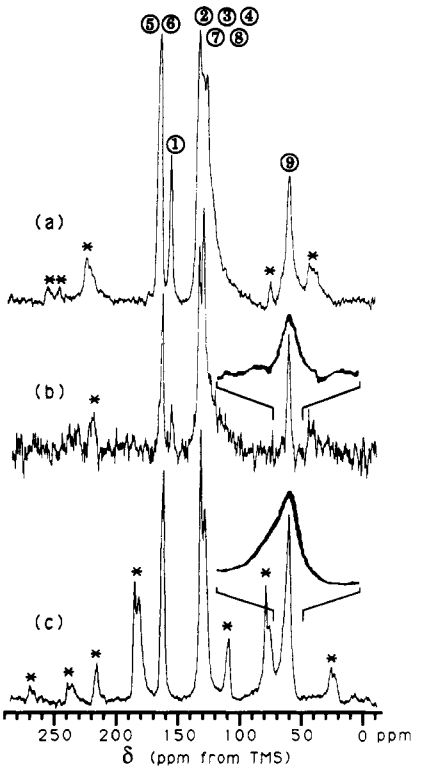

Figure 4. ^{13}C CP MAS spectra of (a) HBA/ETP 60/40, (b) the long-$T_{1\rho}$ component of HBA/ETP 60/40, and (c) PET. Peak assignments are indicated by the circled numbers and the chart in Figure 3. Asterisks indicate spinning sidebands. A 5× expansion of the region containing the aliphatic peak in the long-$T_{1\rho}$ and PET spectra is shown to allow detailed comparison.

61.5 ppm emanating from ethylene units in the all-trans conformation and a broader upfield shoulder from gauche conformations.[16] The aliphatic peak at 62 ppm of the long-$T_{1\rho}$ component of HBA/ETP 60/40 matches the sharp, all-trans component of the aliphatic peak of PET.

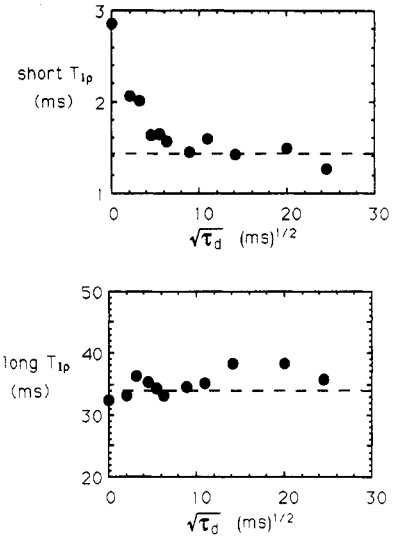

Figure 5. Short and long $T_{1\rho}$ for HBA/ETP 80/20 as a function of the square root of the diffusion time (τ_d). Dashed lines indicate $T_{1\rho}$ values obtained from a spin-lock relaxation experiment at the same spin-lock field strength (5 G).

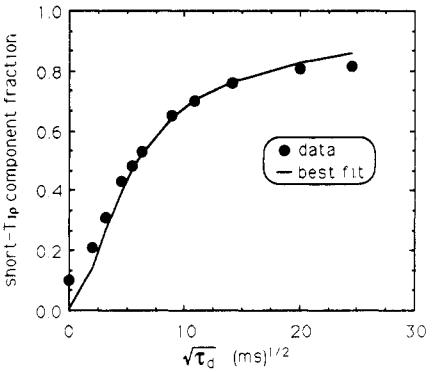

Figure 6. Short-$T_{1\rho}$ component fraction as a function of the square root of the diffusion time (τ_d). The filled circles are the data points and the solid line shows the best fit from the numerical simulation.

This observation, the broad proton line shape, and the long-$T_{1\rho}$ value indicate that this component emanates predominantly from PET-like crystallites.

A minute amount of poly(HBA)-like crystalline phase was also detected in HBA/ETP 60/40. The small peak at 155 ppm seen in Figure 4b indicates the presence of HBA monomer. In additional experiments in which the proton spin-lock time before cross-polarization was increased from 12 ms to values up to 40 ms, this peak decayed with spin-lock time more slowly than the other spectral features, indicating the presence of a very small fraction of poly(HBA)-like crystallites with a very long $T_{1\rho}$. An HBA/ETP 60/40 polymer sample that had been slowly cooled from the melt (10 °C/min from 250 °C) prior to the NMR experiments exhibited an even larger poly(HBA)-like crystalline fraction, although the PET-like crystalline fraction was still predominant.

Proton Spin Diffusion. The characteristic size of the poly(HBA)-like crystallites in HBA/ETP 80/20 was measured by means of a proton spin-diffusion experiment. The spin-lock relaxation data collected in the detection stage of the spin-diffusion experiment were fit to a sum of two exponential decays; the best fit parameters are shown in Figures 5 and 6. Also shown in Figure 6 is the best fit to the data based upon a simulation of the spin-energy transport during the spin-diffusion experiment. The model was used to infer the crystallite size from the spin-diffusion data and will be presented in the Discussion section. The finite amount of spin diffusion at zero

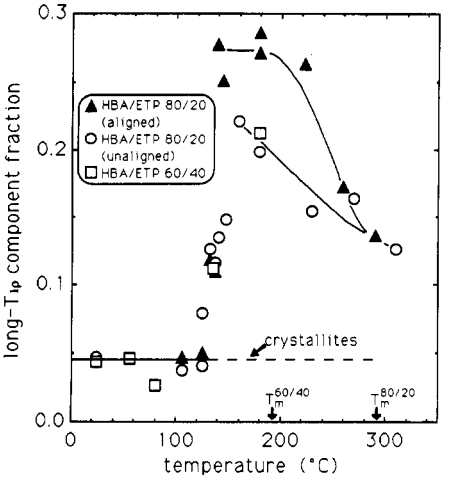

Figure 7. Long-$T_{1\rho}$ component fraction as a function of temperature for HBA/ETP 80/20 (both aligned and unaligned) and HBA/ETP 60/40. Melting points of the two copolymers as determined by Meesiri et al.[1] are indicated.

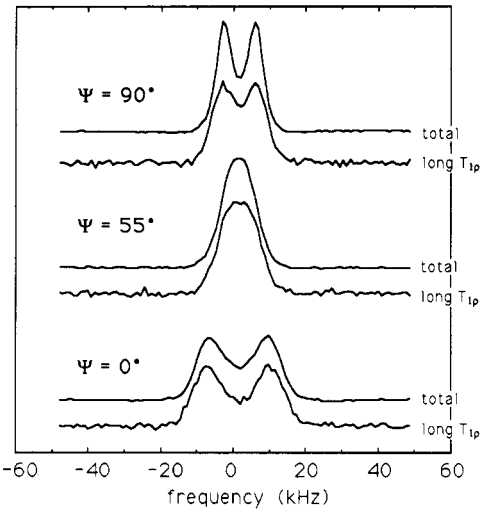

Figure 8. Total and long-$T_{1\rho}$ proton line shapes of an aligned HBA/ETP 80/20 polymer sample at 220 °C for three angles (Ψ) between the alignment direction and the magnetic field. The slightly increased broadening of the long-$T_{1\rho}$ line shapes over the line shapes of the total polymer sample suggests that molecular motion is somewhat more restricted in the long-$T_{1\rho}$ component than in the bulk.

diffusion time indicates that some spin diffusion occurred during the preparation stage of the spin-diffusion experiment.

Elevated-Temperature NMR Experiments and Results

Proton NMR. Above 130 °C, the proton spin-lock relaxation behavior of HBA/ETP 80/20 is again described well by a sum of two exponential decays, but the long-$T_{1\rho}$ fraction is about 22–28% near 130 °C and drops monotonically to about 15% near the polymer melting point (Figure 7). Data from an aligned polymer sample are also shown. (Alignment was achieved by heating the polymer sample to about 40 °C above the melting point for 20 min in the large NMR spectrometer magnetic field. Based upon proton line-shape measurements, the order parameter of the aligned polymer sample was about 0.8.) The aligned and unaligned polymer samples show qualitatively similar spin-lock relaxation behavior. The transition in spin-lock relaxation behavior between 110 and 130 °C is completely reversible. Similar behavior was observed for HBA/ETP 60/40 (Figure 7), although there was insufficient data to define a trend above 130 °C. The remainder of this section describes proton and ^{13}C NMR measurements performed in order to elucidate the nature of molecular dynamics in the short-$T_{1\rho}$ and long-$T_{1\rho}$ components above 130 °C in both copolymers.

Figure 8 shows the bulk and long-$T_{1\rho}$ proton line shapes of an aligned HBA/ETP 80/20 polymer sample at 220 °C. The dominant feature is the symmetric doublet resulting from the dipolar interaction between nearest-neighbor protons on the aromatic rings. Fluctuations of the aromatic rings about their para-substituted axes reduce other intramolecular and intermolecular proton dipolar interactions. The signal from the aliphatic protons is not apparent, presumably due to the fact that aliphatic protons are only 17% abundant and that their line shape is broad. As expected, the aromatic proton spectral splitting scales as $|P_2(\Psi)|$ (the absolute value of the second Legendre polynomial, where Ψ is the angle between the applied magnetic field and the alignment direction).[17,18] Note that the long-$T_{1\rho}$ line shape is very similar to the total line shape for all alignment directions, except that the features are slightly more broadened, suggesting that molecular motion in the long-$T_{1\rho}$ component is somewhat more restricted than in the rest of the polymer.

A dependence of $T_{1\rho}$ on the spin-lock field strength is an indicator of the presence of mid-kilohertz frequency molecular motion.[19] The spin–lock relaxation rates ($1/T_{1\rho}$) of the short- and long-$T_{1\rho}$ components at 270 °C are shown in Figure 9. The decreasing relaxation rate with spin-lock field strength in the short-$T_{1\rho}$ component indicates the presence of a mid-kilohertz frequency molecular motion. This motion is absent in the long-$T_{1\rho}$ component.

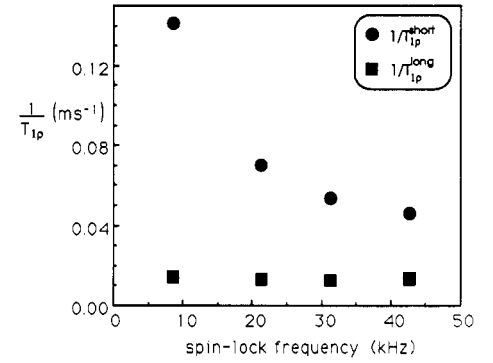

Figure 9. Spin-lock relaxation rate ($1/T_{1\rho}$) as a function of the spin-lock frequency for unaligned HBA/ETP 80/20 at 270 °C.

The spin-lock relaxation behavior of protons in HBA/ETP 80/20 at 220 °C was measured for three orientations of the aligned polymer with respect to the direction of the magnetic field. The polymer sample was rotated by hand approximately 55° and 90° away from the orientation of alignment with the magnetic field; the temperature was sufficiently low that realignment of the polymer sample did not occur. The short-$T_{1\rho}$ exhibits a strong anisotropy (Figure 10), which is strikingly similar to the proton relaxation behavior seen in small-molecule liquid crystals when the dominant relaxation mechanism involves fluctuations of the long molecular axis about the preferred direction of alignment.[20] By analogy it is expected that the mid-kilohertz frequency molecular motion that causes relaxation in the short-$T_{1\rho}$ component is angular fluctuations of the local polymer chain axis. The nature and time scale of this motion suggest that it is cooperative. The lack of any significant anisotropy of the long $T_{1\rho}$, on the other hand, suggests that this motion is absent in the long-$T_{1\rho}$ component.

An Arrhenius plot of the short-$T_{1\rho}$ spin-lock relaxation rate for both copolymers is shown in Figure 11. The

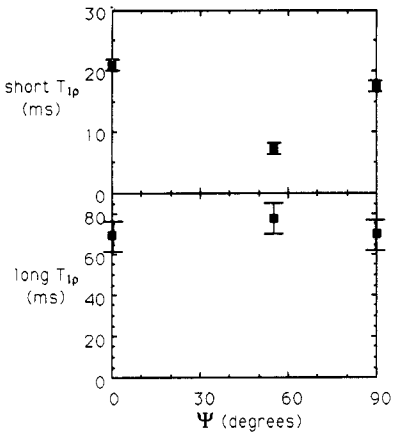

Figure 10. Short- and long-$T_{1\rho}$ values for aligned HBA/ETP 80/20 at 220 °C for the alignment direction at 0, 55, and 90° with respect to the magnetic field.

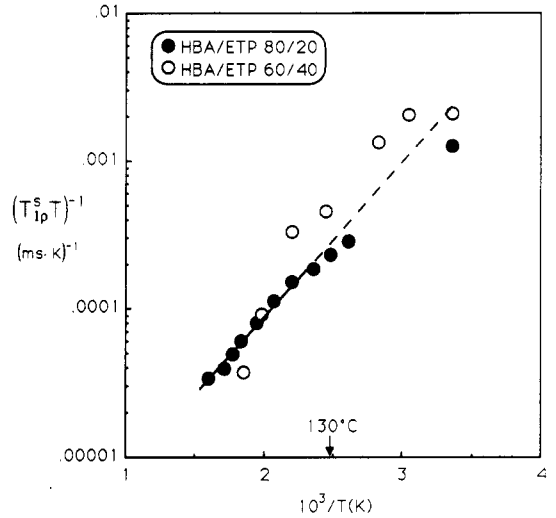

Figure 11. Spin-lock relaxation rate of the short-$T_{1\rho}$ component times inverse temperature versus the inverse temperature for HBA/ETP 80/20 and HBA/ETP 60/40. The best exponential fit to the HBA/ETP 80/20 data above 130 °C is shown (solid line). The slope of this line gives an activation energy of 4.8 kcal/mol for the dominant relaxation mechanism in the short-$T_{1\rho}$ component of the polymer sample. The HBA/ETP 60/40 data above 130 °C could not be described adequately by a single-exponential curve.

abscissa is multiplied by the inverse temperature to account for an expected increase in amplitude of motion with temperature.[21] The data for HBA/ETP 80/20 above 130 °C exhibit Arrhenius behavior with an activation energy of 4.8 kcal/mol. (The slope is positive because the spin-lock relaxation mechanism is in the weak collision limit.[19,22]) The behavior of the data above 130 °C for HBA/ETP 60/40 are more complex; there is an apparent break in the slope around 180 °C, although there are insufficient data for a definitive inference. It is perhaps significant that this is near the temperature at which the nonnematic fraction of this polymer first becomes apparent.[15]

Static ^{13}C NMR. Rapid molecular motion modulates the effect of the chemical shift interaction on the line shape in a predictable way, and thus static ^{13}C spectra contain information about molecular motion. Typically, static ^{13}C spectra are not utilized in the study of unenriched polymers because of the severe overlap of the various line shapes from chemically distinct ^{13}C species. The inhomogeneous line width can be greatly reduced, however, by aligning the polymer samples in the magnetic field as described previously. Figure 12 shows ^{13}C spectra of HBA/ETP 80/20 at 210 °C with the direction of alignment along the

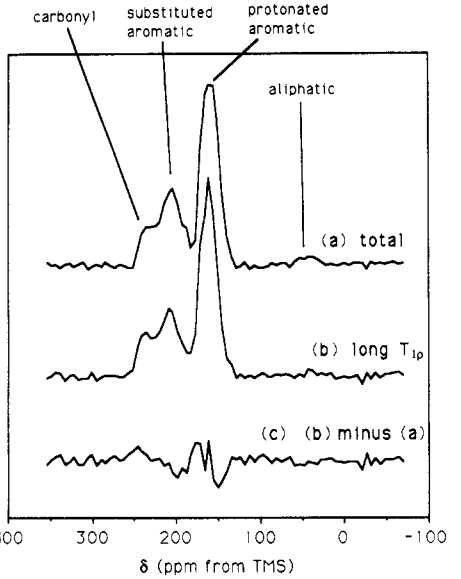

Figure 12. Static ^{13}C spectra of HBA/ETP 80/20 at 210 °C aligned parallel to the magnetic field: (a) the ^{13}C spectrum of the entire polymer sample and (b) the ^{13}C spectrum of the long proton $T_{1\rho}$ component. Both spectra have been normalized. (c) The subtraction of spectrum a from spectrum b. Peak assignments are indicated.

magnetic field. Peak assignments were made, based on previously reported chemical shift data,[23,24] signal strengths, and relative signal strengths between spectra of HBA/ETP 80/20 and HBA/ETP 60/40. Unambiguous assignment of all spectral features is not possible. The substituted aromatic carbon signals cannot be resolved from one another and can be barely resolved from the carbonyl carbon peak. The large protonated aromatic carbon peak at 172 ppm and the aliphatic peak at 42 ppm can be easily resolved, however.

The ^{13}C spectra of both the bulk and the long proton $T_{1\rho}$ component are nearly identical. The subtraction spectrum (Figure 12c) reveals only a slight difference in the two spectra, resulting in a weak peak within a broad well centered at about 170 ppm; this feature indicates that the protonated aromatic carbon signal from the long-$T_{1\rho}$ component is slightly narrower than for the polymer bulk. This narrowing can be explained by a slightly greater degree of alignment of the long-$T_{1\rho}$ component over the bulk, since misalignment results in inhomogeneous broadening of spectral features. This is qualitatively consistent with the absence of cooperative motion in the long-$T_{1\rho}$ component, since cooperative motion reduces the degree of alignment. Analogous results were found for HBA/ETP 60/40 at 130 °C (Figure 13). Since static ^{13}C NMR experiments required 1–3 days to complete, initial ^{13}C measurements and proton spin-lock relaxation measurements were repeated at the end of each sequence to check for microstructural changes during the course of the experiments. No changes were observed.

Figure 14 shows ^{13}C spectra of HBA/ETP 80/20 taken under conditions similar to those for the spectra shown in Figure 12, but with the direction of alignment perpendicular to the magnetic field. Peak assignments were made, based on ^{13}C chemical shift positions for alignment parallel to the magnetic field and the isotropic chemical shifts determined from the ^{13}C MAS NMR experiments (see below) and the relationship

$$\sigma_{\text{isotropic}} = (1/3)(\sigma_{\text{parallel}} + 2\sigma_{\text{perpendicular}}) \quad (1)$$

where σ_{parallel} and $\sigma_{\text{perpendicular}}$ are the chemical shifts for alignment parallel and perpendicular to the magnetic field. This relation is valid when the alignment of the polymer

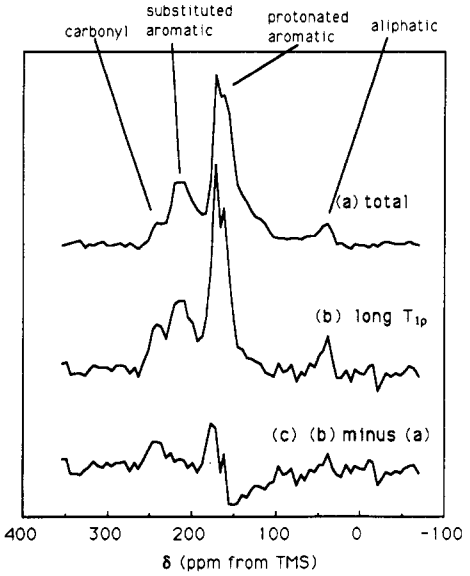

Figure 13. Static ^{13}C spectra of HBA/ETP 60/40 at 130 °C aligned parallel to the magnetic field: (a) the ^{13}C spectrum of the entire polymer sample and (b) the ^{13}C spectrum of the long proton $T_{1\rho}$ component. Both spectra have been normalized. (c) The subtraction of spectrum a from spectrum b.

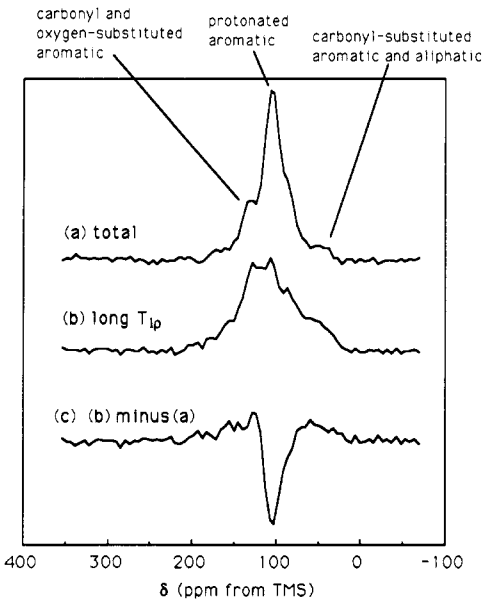

Figure 14. Static ^{13}C spectra of HBA/ETP 80/20 at 210 °C aligned perpendicular to the magnetic field: (a) the ^{13}C spectrum of the entire polymer sample and (b) the ^{13}C spectrum of the long proton $T_{1\rho}$ component. Both spectra have been normalized. (c) The subtraction of spectrum a from spectrum b.

sample is strong and there is rapid rotational motion of polymer chain segments about the polymer chain axis. (It will be shown that the second condition is the case only for the short-$T_{1\rho}$ component of the polymer samples.) The protonated aromatic carbon peak of the polymer bulk is now at 112 ppm. This peak has the same line width as in Figure 12a, indicating that the aromatic rings experience rapid isotropic motion about their substituted axes, as will be explained in the Discussion section. The protonated aromatic carbon peak of the long proton $T_{1\rho}$ component, however, is significantly broadened (Figure 14b). From the difference spectrum (Figure 14c), the inhomogeneous line width of the protonated aromatic carbon line shape of the long-$T_{1\rho}$ component was determined to be 124 ± 20 ppm. Assuming that the line shape is close to Gaussian in shape, the square root of the second moment of the line shape is 53 ± 8 ppm. Nearly identical results were obtained for HBA/ETP 60/40 at 130 °C (Figure 15).

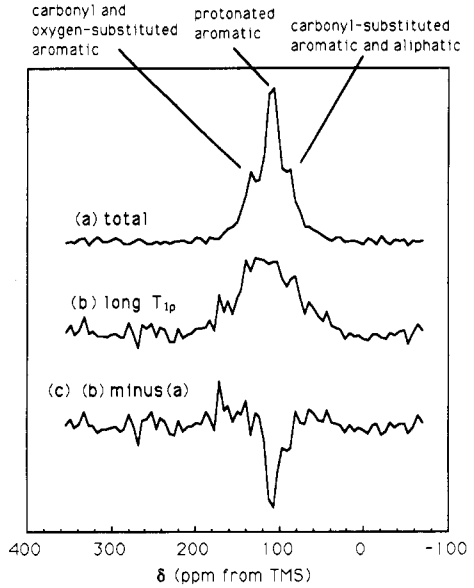

Figure 15. Static ^{13}C spectra of HBA/ETP 60/40 at 130 °C aligned perpendicular to the magnetic field: (a) the ^{13}C spectrum of the entire polymer sample and (b) the ^{13}C spectrum of the long proton $T_{1\rho}$ component. Both spectra have been normalized. (c) The subtraction of spectrum a from spectrum b.

In the Discussion section, this broadening will be explained in terms of restriction of aromatic ring motion in the long-$T_{1\rho}$ component.

Elevated-Temperature ^{13}C CP MAS NMR. The elevated-temperature ^{13}C CP MAS spectra of HBA/ETP copolymers have two uses in this study. First, knowledge of the isotropic chemical shift values of the various ^{13}C species obtained from these spectra was used to assign features of the static ^{13}C spectra (via eq 1). Second, because of the well-separated features and high signal-to-noise ratio of MAS spectra, the HBA mole fraction of the long proton $T_{1\rho}$ regions could be easily determined. Figure 16a shows the ^{13}C CP MAS spectrum of HBA/ETP 80/20 at 210 °C. Peak assignments were made by using the ^{13}C NMR spectrum of PET (see Figure 4), the ^{13}C spectrum of poly(HBA),[25] relative magnitudes of peaks, and differences in peak heights between the spectrum of HBA/ETP 80/20 and HBA/ETP 60/40. The ^{13}C MAS spectrum of the long proton $T_{1\rho}$ regions (Figure 16b) was obtained by spin locking the proton magnetization for 64 ms prior to a 3-ms cross-polarization using a 5-G spin-lock field. The long proton $T_{1\rho}$ spectrum was scaled so that the largest peak (at 131.3 ppm) had the same magnitude as in the bulk spectrum; the resultant spectrum was subtracted from the bulk spectrum to give the subtraction spectrum shown in Figure 16c. The subtraction spectrum shows features at 123.0, 163.9, and 171.5 ppm. The peaks at 163.9 and 171.5 ppm are at spinning sideband positions, and their presence reflects an apparent slight difference in the sample spinning speed during collection of the two spectra or a difference in the size of the residual chemical shift anisotropy for carbons in the short- and long-$T_{1\rho}$ components. For an unknown reason, the peak at 122.2 ppm was found to be shifted by about 1 ppm in the long-$T_{1\rho}$ spectrum. This shift manifests itself in the subtraction spectrum as a feature with no net area. However, the absence of residual mass at the positions of parent peaks corresponding to the ETP monomer indicates that the monomer fraction in the long proton $T_{1\rho}$ component is the same as in the bulk, within uncertainty. The uncertainty in the stoichiometry of the long proton $T_{1\rho}$ phase is dominated by the noise in the long proton $T_{1\rho}$ spectrum and is about ±19%. Thus, it can be determined that the

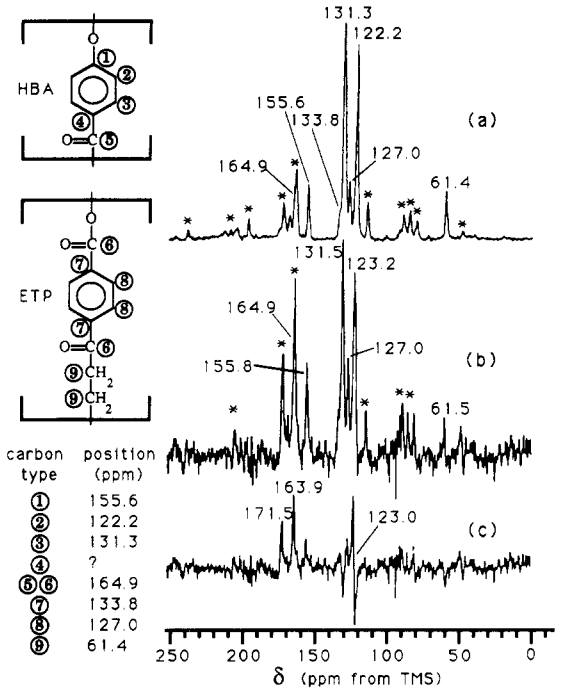

Figure 16. (a) Total and (b) long proton $T_{1\rho}$ ^{13}C CP MAS spectra of HBA/ETP 80/20 at 210 °C. (c) Subtraction spectrum ((a) minus (b)), where a scaling factor was applied to (b) so that subtraction of the peaks at 131.3 ppm gave no residue. Numbers indicate chemical shifts and asterisks indicate spinning sidebands. Peak assignments for spectrum a are indicated by the circled numbers and the charts to the left.

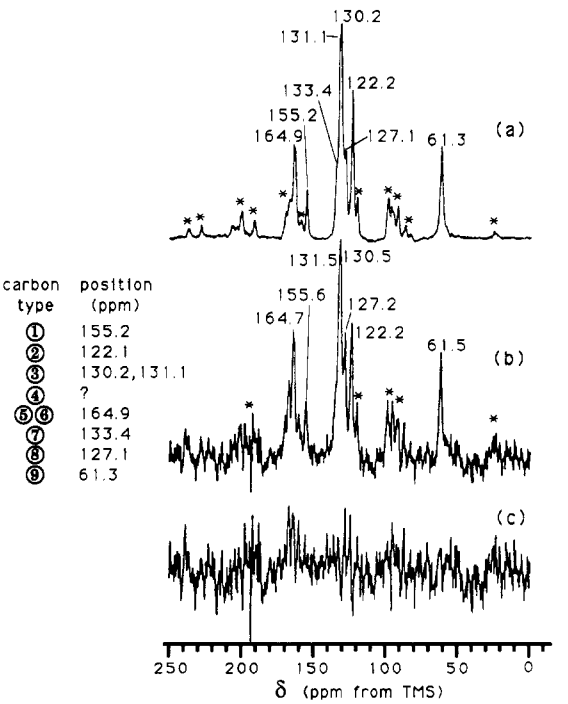

Figure 17. (a) Total and (b) long proton $T_{1\rho}$ ^{13}C CP MAS spectra of HBA/ETP 60/40 at 130 °C. (c) The subtraction spectrum ((a) minus (b)), where a scaling factor was applied to (b) so that subtraction of the peaks at 130.2 ppm gave no residue. Numbers indicate chemical shifts and asterisks indicate spinning sidebands. Peak assignments for spectrum a are indicated by the chart to the left and the diagram in Figure 16.

long proton $T_{1\rho}$ component has an HBA monomer fraction of 0.80 ± 0.15.

Figure 17a,b show the bulk and long proton $T_{1\rho}$ CP MAS ^{13}C spectra of HBA/ETP 60/40 at 130 °C. The long proton $T_{1\rho}$ spectrum was obtained by using a 16-ms proton spin lock with a 5-G spin-lock field prior to the 3-ms cross-polarization. The 130.2-ppm peak height was used to normalize the two spectra (as with Figure 16), which were then subtracted to yield the subtraction spectrum shown in Figure 17c. The absence of features in the subtraction spectrum indicate that the HBA monomer fraction of the long proton $T_{1\rho}$ component is the same as for the total polymer sample. The uncertainty in the HBA mole fraction, based on the noise level of the long-$T_{1\rho}$ spectrum, is ±6%. Thus, the long proton $T_{1\rho}$ component has an HBA monomer fraction of 0.60 ± 0.04.

Discussion

Investigation of Crystallites. Room Temperature Spin-Lock Relaxation and ^{13}C CP MAS NMR. All of the proton and ^{13}C NMR results for HBA/ETP 80/20 below 110 °C are consistent with the assignment of the long-$T_{1\rho}$ component to a poly(HBA)-like crystalline phase. The broad proton line shape of the long-$T_{1\rho}$ component, which does not narrow with increasing temperature, is consistent with a rigid domain, and the ^{13}C spectrum identifies this component as a poly(HBA)-like crystalline phase. This interpretation is consistent with the observation made by Zachariades and co-workers[2] of poly(HBA)-like lamellar structures in HBA/ETP 80/20. The crystalline fraction as measured by spin-lock relaxation was insensitive to quenching or slow cooling from the melt.

Similar proton NMR results were obtained for HBA/ETP 60/40, but in this case, the ^{13}C NMR spectra clearly identify the long-$T_{1\rho}$ component as predominantly PET-like crystallites. A very small amount of poly(HBA)-like crystallites was also detected. These observations are consistent with the melting point data for HBA/ETP copolymers, which indicate that for HBA-rich compositions the dominant crystalline form is poly(HBA)-like, while for ETP-rich compositions the dominant crystal form is PET-like, with a crossover point near the 60/40 composition.[1] This trend is also supported by X-ray diffraction.[13]

Although slow cooling or quenching from the melt had no detectable effect on the poly(HBA)-like crystalline fraction in HBA/ETP 80/20, slow cooling of the HBA/ETP 60/40 polymer sample from the melt did result in an increase in the small amount of poly(HBA)-like crystallites, although the PET-like crystalline fraction was still predominant.

Proton Spin-Diffusion Simulation. It is characteristic of diffusion experiments that the shortest linear dimension across which diffusion occurs is relatively easy to determine, but more detailed geometric information, such as shape or size dispersion, is difficult to infer. The "fuzziness" of spin gradients created during the preparation stage of the spin-diffusion experiments further limits the obtainable information, and at best a crystallite length scale can be extracted. Thus, the spin-diffusion simulation must be based upon a model for which the crystallite geometry is assumed, and only the crystallite size and mass fraction are varied in order to find agreement with the spin-diffusion data.

Electron microscopy work by Zachariades and co-workers[2] revealed poly(HBA)-like crystalline structures in HBA/ETP 80/20 in the form of platelets. The crystallite geometry model chosen for our simulation is a simplification based upon this observation, namely, a periodic array of planar crystallites of infinite extent in two dimensions and a finite thickness in the third (Figure 18). The spacing between crystallites in the model is made uniform. This model is chosen because it reduces the spin energy transport equation to a one-dimensional equation within a finite unit cell, while retaining the important physical characteristics.

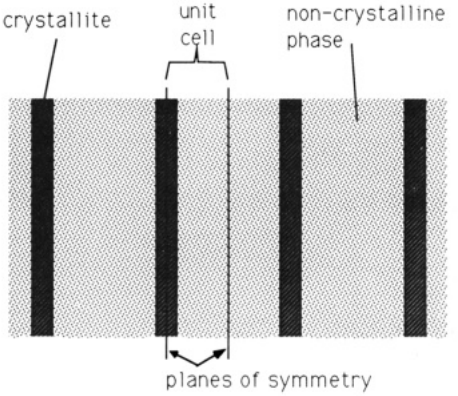

Figure 18. Simple model for crystallite geometry. Crystallite sheets are of infinite extent in two dimensions and are arranged in an infinite periodic array in the third dimension. The primitive cell boundary planes are indicated by solid lines.

In each diffusion experiment step, the spin energy transport equation is of the form

$$dm(\mathbf{x},t)/dt = \nabla\cdot[\mathbf{D}(\mathbf{x})\nabla m(\mathbf{x},t)] - \frac{1}{T(\mathbf{x})}[m(\mathbf{x},t) - m_{eq}] \quad (2)$$

where $m(\mathbf{x},t)$ is the nuclear magnetization density as a function of position ($\mathbf{x}$) and time (t), $D(\mathbf{x})$ is the diffusion coefficient for spin energy, $1/T(\mathbf{x})$ is the local intrinsic spin–lattice relaxation rate, and m_{eq} is the equilibrium magnetization. During the preparation and detection steps the proton magnetization is spin-locked, so m_{eq} is very close to zero and T equals $T_{1\rho}$. $T_{1\rho}$ of the noncrystalline phase protons is known from the spin-lock relaxation data. The intrinsic $T_{1\rho}$ of the crystalline phase protons was assumed to be much larger than the diffusion time scale (the square of the crystallite half-thickness divided by D), based on the fact that the long $T_{1\rho}$ of protons in poly(HBA), which is mostly crystalline, was measured to be 120 ms.[15] (The $T_{1\rho}$ value of 33 ms associated with the crystalline phase of HBA/ETP 80/20 is due to spin diffusion out of the crystalline phase into the noncrystalline phase and does not reflect the intrinsic spin-lock relaxation of the crystalline phase.) For the diffusion stage, m_{eq} equals the equilibrium magnetization strength in the absence of resonant irradiation, and T equals T_1, which is 1.3 s[15] in the noncrystalline phase. The intrinsic T_1 of the crystalline phase is presumably at least as large as T_1 of poly(HBA), which is much larger than the experimental time scale.[15] The diffusion coefficient was estimated to be 5×10^{-12} cm^2/s in both the crystalline and noncrystalline phases by using the diffusion coefficient for PET determined by Havens and VanderHart[26] and the proton densities of HBA/ETP copolymers and PET and by assuming that the diffusion coefficient scales as the proton density to the one-third power.[27] Because spin locking partially averages the homonuclear proton dipolar interactions, the diffusion coefficient in the limit of strong spin locking is one-half this value[22] and between unity and one-half this value for the spin-lock strength used in these experiments.[19,22] Also, it was assumed that the diffusion coefficient was isotropic and independent of position.

The transport equation (2) was discretized in space and solved on a grid of 100 equally spaced points across a unit cell using discrete time stepping. Symmetry boundary conditions were imposed at each end of the cell. The crystalline fraction and the crystallite thickness were varied until both the spin-lock relaxation data and the spin-diffusion results could be consistently reproduced. The best fit to the spin-diffusion data (shown in Figure 6) is given by a simulation where the crystallite thickness is 80 Å and the crystallite mass fraction is 5%. Note that the simulation indicates that the crystallite fraction of ~5% inferred from the two-exponential fit to the spin-lock relaxation data is a reasonable value even after spin diffusion is taken into account. Deviations between the simulation and experimental data at short and long diffusion times are probably due to crystallite size dispersion and nonuniform distribution, which is not accounted for in the simulation.

Another interesting observation was the anomalously large short-$T_{1\rho}$ value at short spin-diffusion times (see Figure 5). This can be attributed to a boundary layer at the crystallite surfaces where molecular motion in the noncrystalline phase is inhibited by the crystallites. Perhaps this is due to the tight packing of chains in the crystallites. For short diffusion times, the proton magnetization will have diffused into the noncrystalline phase a distance on the order of $(4D\tau)^{1/2}$, where τ is the diffusion time. On the basis of the diffusion coefficient estimate during spin locking ($\sim 3 \times 10^{-12}$ cm^2/s, determined by the simulation of the data) and the time scale of the $T_{1\rho}$ enhancement (~10 ms), the boundary layer is estimate to be about 30 Å thick.

Elevated-Temperature Spin-Lock Relaxation. The goal of the elevated-temperature work was to develop an understanding of molecular dynamics associated with the glass transitions of HBA/ETP copolymers. Thermal analysis indicates two glass transitions in both copolymers:[1,28] a lower glass transition at 66 °C in HBA/ETP 80/20 and at 85 °C in HBA/ETP 60/40 and an upper glass transition at 183 °C in HBA/ETP 80/20 and at 167 °C in HBA/ETP 60/40. Dielectric relaxation spectroscopy has also been used to investigate the lower glass transition.[6,7] In this Discussion, it will be argued that the NMR spin-lock relaxation in both copolymers above 110 °C is induced primarily by motion associated with deglassification.

Below 110 °C, spin-lock relaxation easily distinguishes a ~5% signal from homopolymer-like crystallites. About 110 °C, the long-$T_{1\rho}$ component fraction of HBA/ETP 80/20 rises to much larger values, between 22 and 28%. This rise is reversible and so is not a result of irreversible morphological changes such as annealing. The elevated-temperature proton line shapes of the long-$T_{1\rho}$ component are similar to the bulk line shapes, although their features are slightly broader than those of the bulk line shapes (Figure 8). This indicates that the elevated-temperature long-$T_{1\rho}$ component is not a tightly bound crystalline structure, but molecular motion is more restricted than in the rest of the polymer. A more quantitative conclusion can be drawn from analysis of the ^{13}C data, as is discussed below. Also, a spin-diffusion experiment identical with the one described earlier was performed on HBA/ETP 80/20 at 160 °C, with a maximum diffusion time of 100 ms. No spin diffusion was observed, indicating that the proton magnetization in the elevated-temperature short- and long-$T_{1\rho}$ components are not coupled via spin diffusion on the time scale of the spin-lock relaxation experiment. This is in contrast to the room temperature behavior, where spin diffusion was the dominant mode of relaxation of the long-$T_{1\rho}$ magnetization.

Several proton spin-lock relaxation measurements were made on HBA/ETP 80/20 to further characterize the dominant spin–lattice relaxation mechanism in the short-$T_{1\rho}$ component. The fact that the spin-lock relaxation rate in the short-$T_{1\rho}$ component decreased with spin-lock frequency indicates that the dominant relaxation mechanism exhibits a correlation frequency in the mid-kilohertz range.[19] This motion is absent in the long-$T_{1\rho}$ component, where the relaxation rate is small and independent of the spin-lock frequency.

The angle dependence of the short-$T_{1\rho}$ spin-lock relaxation time of protons in HBA/ETP 80/20 is striking (Figure 10); $T_{1\rho}$ varied by a factor of about 3 between 0° and 55° orientations. A quantitatively similar anisotropy is also seen for proton spin–lattice relaxation in small-molecule liquid crystals when the dominant relaxation mechanism involves thermal fluctuations of the molecular long axis about its preferred alignment direction.[20] Such a relaxation mechanism is predominant for many small-molecule liquid crystals.[20] The essential ingredients giving rise to the strong anistropy are rapid rotational fluctuations of the molecule about a special "long axis" and slow fluctuations of the long axis about a preferred orientation. The former motion rapidly averages the dipolar couplings so that the residual interactions all have principal axes along the direction of the long axis. This uniformity gives rise to the strong anisotropy of the relaxation rate. The latter motion is responsible for spin–lattice relaxation. By analogy, it is inferred that the molecular motion giving rise to spin-lock relaxation in HBA/ETP copolymers above 130 °C is a cooperative motion that involves rapid rotational fluctuations of polymer chain segments about the local polymer chain axis and slower small-amplitude angular fluctuations of the polymer chain axis about the local nematic director. This motion is absent in the long-$T_{1\rho}$ component.

Takase and co-workers[7] and Gedde and co-workers[6] used dielectric relaxation spectroscopy to study the lower glass transition of HBA/ETP copolymers. Using the characterization by Gedde and co-workers, the α and β processes associated with the lower glass transition should merge at about 80 °C, above which the glass transition process should exhibit an activation energy close to that of the β process, about 5 kcal/mol. This activation energy is close to the 4.8 kcal/mol activation energy of the molecular motion associated with the short-$T_{1\rho}$ spin-lock relaxation mechanism. This strengthens the connection between the lower glass transition as observed by dielectric spectroscopy and the dominant short-$T_{1\rho}$ spin-lock relaxation mechanism above 130 °C. This is also consistent with the characterization of the mid-kilohertz frequency motion in the previous paragraph.

Generally, a "$T_{1\rho}$ minimum" is observed near a glass transition. Perhaps the reason one is not observed for these copolymers is that, below 110 °C, a different relaxation mechanism is dominant (as evidenced by the different activation energy seen below 110 °C). This mechanism probably involves intermolecular dipolar couplings. If the $T_{1\rho}$ minimum associated with cooperative motion is below 110 °C, it could be obscured by the dominance of the competing intermolecular relaxation mechanism.

Static ^{13}C NMR. The protonated aromatic carbon peak is the dominant feature in the static ^{13}C spectra and thus will be the focus of analysis. The inhomogeneous broadening of this peak can be estimated from knowledge of the chemical shift tensor. We assume that the chemical shift principal values of these carbons in the HBA and ETP monomer are the same as for the aromatic carbons of PET, specifically 226, 153, and 15 ppm, as determined by Murphy and co-workers.[23] The chemical shift principal axis system for aromatic ring carbons is assumed to have the axis of largest shielding perpendicular to the aromatic ring and the axis of least shielding along the carbon-substituent bond. These assumptions are supported by the fact that they correctly predict the positions of the protonated aromatic carbon peak of the aligned polymer samples at both orientations. Using the chemical shift tensor defined by these numbers and directions, the chemical shift of the protonated aromatic carbons as a function of the orientation of the aromatic ring is

$$\sigma_{zz}(\theta,\phi) = (171 - 60\sin^2\theta - 63\sin\theta\cos\theta\sin\phi - 96\sin^2\theta\cos 2\phi)\ \text{ppm} \quad (3)$$

where θ is the angle between the aromatic ring substituted axis and the applied magnetic field and ϕ is the angle of rotation of the aromatic ring plane about the substituted axis (ϕ equal to zero corresponds to the orientation for which the ring plane is perpendicular to the magnetic field when θ equals $\pi/2$).

In this analysis, we assume that the substituted axes of the aromatic rings are parallel to the direction of alignment in a well-oriented polymer sample. This is only approximately correct because of imperfect macroscopic alignment of polymer chains in aligned samples and because the substituted axes are not exactly parallel to the local chain axis.[29] Estimates show that errors due to these effects should be small, however.

In the case of alignment of the polymer sample parallel to the magnetic field, θ equals zero and eq 3 gives

$$\sigma_{zz}(0,\phi) = 171\ \text{ppm} \quad (4)$$

Note that for this orientation the chemical shift is independent of the angle ϕ, and thus there is no inhomogeneous broadening of the protonated aromatic carbon peak. The consequence of this is the relatively narrow peak for these carbons as seen in Figures 12 and 13. For orientation perpendicular to the magnetic field, θ equals $\pi/2$ and the chemical shift is

$$\sigma_{zz}\left(\frac{\pi}{2},\phi\right) = (111 - 96\cos 2\phi)\ \text{ppm} \quad (5)$$

The ϕ-dependence of σ_{zz} for this orientation indicates significant inhomogeneous broadening. From this equation and the formula

$$(\Delta\sigma)^2 = \frac{1}{2\pi}\int_0^{2\pi}(\sigma(\phi) - \langle\sigma\rangle)^2\,d\phi \quad (6)$$

where $\Delta\sigma$ is the square root of the second moment of the line shape and $\langle\sigma\rangle$ is the chemical shift averaged over all angles ϕ, $\Delta\sigma$ is found to be 68 ppm.

This anticipated broadening for the case of perpendicular alignment is clearly not present in the short-$T_{1\rho}$ component, since the line width of the aromatic carbons for perpendicular orientation is about the same as for parallel orientation and is much smaller than 68 ppm (see Figures 12a–15a). Instead, the inhomogeneous broadening in the case of perpendicular alignment must be reduced by fast rotation of the aromatic rings about their substituted axes.

For the long-$T_{1\rho}$ component, however, the line width for perpendicular alignment is significantly broader than for parallel alignment (see Figures 12b–15b). On the basis of the width of the broad peak in the subtraction spectrum for HBA/ETP 80/20, the inhomogeneous broadening is 53 ± 8 ppm, which is on the order of, but less than, the predicted value of 68 ppm. The most likely explanation for the small reduction of the inhomogeneous broadening from the expected static value is small-angle aromatic ring fluctuations about their substituted axes. A simple model for such motion is one in which the orientation angle ϕ of a particular aromatic ring fluctuates about an equilibrium angle ϕ_0. The exact shape of the time-averaged probability distribution of aromatic ring orientations is not important for this analysis, so a model is used in which the time-averaged probability distribution for an indi-

vidual ring, $P(\phi)$, is Gaussian about ϕ_0 with a half-width ϵ:

$$P(\phi) = \frac{1}{(2\pi)^{1/2}\epsilon} \exp\left[-\frac{1}{2}\left(\frac{\phi - \phi_0}{\epsilon}\right)^2\right] \quad (7)$$

This distribution is physically reasonable for small-amplitude fluctuations ($\epsilon \ll \pi$). On the basis of this model, the time-averaged chemical shift is

$$\bar{\sigma}(\phi_0;\epsilon) = (111 - 96\ \overline{\cos 2\phi}) \text{ ppm} = (111 - 96e^{-2\epsilon} \cos 2\phi_0) \text{ ppm} \quad (\epsilon \ll \pi) \quad (8)$$

Here, the bar indicates a time average over fast orientational fluctuations. From this expression and eq 6, where $\sigma(\phi)$ has been replaced by $\bar{\sigma}(\phi_0;\epsilon)$, the inhomogeneous contribution to the line width $\Delta\sigma$ is

$$\Delta\sigma = 68e^{-2\epsilon^2} \text{ ppm} \quad (\epsilon \ll \pi) \quad (9)$$

Equating this expression with the observed value of 53 ± 8 ppm yields a value for ϵ of 20 ± 6°. The static ^{13}C NMR line shapes were nearly identical for HBA/ETP 60/40 at 130 °C, and thus this conclusion applies to the long-$T_{1\rho}$ component of that copolymer as well. Whether or not the aromatic rings in the long-$T_{1\rho}$ component also undergo 180° flips cannot be ascertained from the static ^{13}C NMR data, since for the cases of parallel alignment ($\theta = 0$) or perpendicular alignment ($\theta = 90°$), the chemical shift is invariant with respect to 180° flips (see eq 3).

Recall also that the proton line shapes of the long-$T_{1\rho}$ component of HBA/ETP 80/20 at 220 °C (Figure 8) reveal that the intermolecular and cross-ring dipolar couplings are weak but are larger than in the short-$T_{1\rho}$ component. This observation is explained by the presence of the above-mentioned small-amplitude angular fluctuations. Such fluctuations would significantly reduce, but not eliminate, those dipolar couplings, while not affecting the dominant nearest-neighbor intramolecular proton couplings.

The constraint of the aromatic ring rotation in the elevated-temperature, long-$T_{1\rho}$ component must be caused by interchain interactions; the presence of aromatic ring fluctuations argues, however, that this long-$T_{1\rho}$ component cannot be predominantly crystalline. Numerous researchers have offered explanations for a rigid, amorphous component in semicrystalline polymers, either as tie chains between crystallites or as polymer chains in the amorphous phase in the vicinity of crystallites (e.g., refs 26, 30, and 31). For the situation at hand, the former scenario would only explain the absence of cooperative motion and not the restriction of aromatic ring rotation in the long-$T_{1\rho}$ component. The latter scenario would explain the restricted aromatic ring motion, however. Chain reentry at the crystallite surface would be prohibited by the stiffness of the polymer chains, thus the crystal-type chain packing would be imposed upon the polymer chains for some distance after they have left the crystallite surface. Such a scenario is illustrated in Figure 19. The long-$T_{1\rho}$ component includes the crystalline phase plus a "domain of influence" of the crystallites within which aromatic ring rotations would be inhibited. Given this scenario, since the crystalline fraction and the elevated-temperature long-$T_{1\rho}$ component fraction are known from spin-diffusion and spin-relaxation experiments, the composition of the elevated-temperature long-$T_{1\rho}$ components can be easily predicted. It should be 86 mol % HBA for HBA/ETP 80/20 and 43 mol % HBA for HBA/ETP 60/40 at the respective temperatures at which the ^{13}C MAS spectra were collected. The ^{13}C MAS spectra clearly rule out the predicted composition for the long-$T_{1\rho}$ component of HBA/ETP 60/40; the uncertainty in the ^{13}C MAS data for HBA/ETP 80/20 is too great to make a definitive statement for that copolymer. However, because of the strong similarities in the elevated-temperature long-$T_{1\rho}$ components of the two copolymers, this scenario is effectively ruled out for HBA/ETP 80/20 as well.

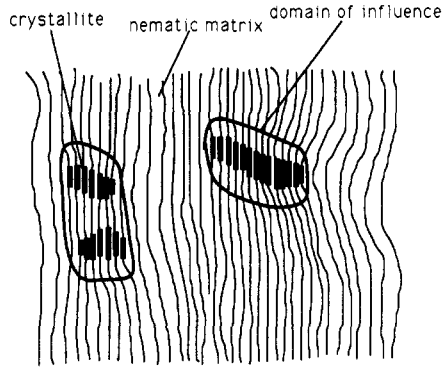

Figure 19. Scenario in which the homopolymer-like crystallites restrict cooperative motion within the surrounding polymer matrix. Crystallites are indicated by heavy lines, and their domains of influence are indicated by the closed loops.

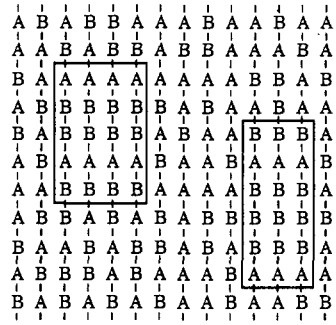

Figure 20. Random copolymers are represented in this figure by random sequences of two monomers (denoted A and B) on polymer chains depicted by vertical lines. In the NPL crystallite scenario, random sequences on neighboring chains find matches (indicated by the rectangles), to form NPL crystallites.

An alternative scenario, which we offer as a speculation, is that the elevated-temperature long-$T_{1\rho}$ components in both copolymers are nonperiodic layer (NPL) crystal structures. This concept was first proposed by Windle and co-workers[32] in order to explain optical measurements on HBA/ETP 60/40. NPL crystals would form when matches of random monomer sequences between neighboring chains are made. Transverse to the local nematic director, the local intermolecular correlation function is that of a crystalline phase, but randomness exists in the direction of the chain axes (Figure 20), and so this phase is pseudocrystalline. Interchain interactions would inhibit cooperative motion within NPL crystallites, and such structures would be expected to have a stoichiometry similar to the bulk composition, as is observed in the long-$T_{1\rho}$ component of both HBA/ETP copolymers. It is likely that the NPL crystals would have to be loosely packed, since the crystal structures of poly(HBA) and PET are incommensurate. This would allow for some motion of the aromatic rings, although that motion would be restricted, as is observed. The reduction of the long-$T_{1\rho}$ component fraction with increasing temperature between 130 °C and the polymer melting point could then be interpreted as gradual melting of NPL crystal structures.

The presence of small poly(HBA)-like crystallites and NPL crystals is also consistent with the steady and time-dependent rheological measurements on the HBA/ETP 80/20 material at 300 °C and above by Kalika and coworkers.[14] Poly-HBA crystallites would persist at the melt temperatures studied, and the presence of submicrome-

ter particles at volume fractions as low as 5% is known to cause shear thinning in otherwise constant-viscosity polymeric liquids. Hence this could be the cause of the unusual power law behavior, which persists over more than eight decades of shear rate. The transient increase of the storage modulus at 300 °C, which is reversible and repeatable following a short temperature excursion to 320 °C, can be explained by the growth and subsequent melting of NPL crystals.

Although the "NPL crystal" scenario perhaps best explains all of the observations associated with the elevated-temperature long-$T_{1\rho}$ component, evidence for such structures is merely circumstantial. Direct evidence would involve measurements of the interchain monomer correlation function, which is unfeasible by the methods presented in this paper.

Conclusions

Microstructure and molecular dynamics of HBA/ETP 80/20 and HBA/ETP 60/40 were studied by solid-state proton and ^{13}C NMR spectroscopy. The HBA/ETP 80/20 copolymer possesses structures resembling poly(HBA) crystallites, with a mass fraction of 4–7% and a smallest linear dimension of about 80 Å. At 24 °C, a ~30 Å boundary layer just outside crystallite surfaces was found within which molecular motion is inhibited, as evidenced by a decrease in the spin-lock relaxation rate within that region. In contrast, the dominant crystal structures in HBA/ETP 60/40 resemble PET crystallites and are about 4–5% abundant. Poly(HBA)-like crystallites were also observed in HBA/ETP 60/40. Their mass fraction increased upon slow cooling from the melt, although PET-like crystallites remained predominant.

Above 130 °C and below the polymer melting temperatures, spin-lock relaxation was shown to be sensitive to cooperative motion involving small angular fluctuations of the local polymer chain axis about the local nematic director. The activation energy associated with this motion is ~4.8 kcal/mol, similar to the activation energy of motion associated with the lower glass transition (at temperatures beyond which the α and β processes converge) as measured by dielectric spectroscopy.[6] Proton NMR spin–lattice relaxation measurements of both copolymers reveal a dominant, short-$T_{1\rho}$ component, which exhibits this cooperative motion, and a minority, long-$T_{1\rho}$ component, which does not exhibit cooperative motion and exhibits slightly better alignment with the magnetic field in aligned samples. The mass fraction of the minority phase in HBA/ETP 80/20 is about 22–28% at 130 °C, dropping to about 15% near the polymer melting point. The mass fraction of the minority phase in HBA/ETP 60/40 is similar, but a trend could not be determined because of insufficient data. Static ^{13}C line shapes revealed that within the short-$T_{1\rho}$ component, the aromatic rings exhibit free rotation about the polymer chain axis, while the aromatic rings exhibit small-angle (~20°) fluctuations about their substituted axes in the long-$T_{1\rho}$ component. ^{13}C MAS NMR showed that the compositions of the long-$T_{1\rho}$ components in both copolymers are the same as the bulk compositions, although the uncertainty in this result is large for HBA/ETP 80/20. Several scenarios to explain the elevated-temperature long-$T_{1\rho}$ component were considered. It was speculated that this component could be NPL crystallites, especially because of the similarity in the monomer mole fractions of the short- and long-$T_{1\rho}$ components. The NMR results would then indicate that the NPL crystallites gradually melt with increasing temperature. More studies would be needed, however, before any such claim could be made definitive.

Acknowledgment. We thank Dr. Grant Haddix for performing the high-temperature magic angle spinning NMR experiments described in this paper and Tennessee Eastman Co. for providing polymer samples. This work was supported by the Director, Office of Energy Research, Office of Basic Energy Sciences, Materials Science Division of the U.S. Department of Energy under Contract DE-AC03-76SF00098 and by a gift from Raychem Corp.

References and Notes

(1) Meesiri, W.; Menczel, J.; Gaur, U.; Wunderlich, B. *J. Polym. Sci., Polym. Phys. Ed.* **1982**, *20*, 719.
(2) Zachariades, A. E.; Economy, J.; Logan, J. A. *J. Appl. Polym. Sci.* **1982**, *27*, 2009.
(3) Blackwell, J.; Lieser, G.; Gutierrez, G. A. *Macromolecules* **1983**, *16*, 1418.
(4) Saywer, L. C. *J. Polym. Sci., Polym. Lett. Ed.* **1984**, *22*, 347.
(5) Joseph, E.; Wilkes, G. L.; Baird, D. G. *Polymer* **1985**, *26*, 689.
(6) Gedde, U. W.; Buerger, D.; Boyd, R. H. *Macromolecules* **1987**, *20*, 988.
(7) Takase, Y.; Mitchell, G. R.; Odajima, A. *Polym. Commun.* **1986**, *27*, 76.
(8) Macfarlane, F. E.; Nicely, V. A.; Davis, T. G. *Contemp. Top. Polym. Sci.* **1977**, *2*, 109.
(9) Nicely, V. A.; Dougherty, J. T.; Renfro, L. W. *Macromolecules* **1987**, *20*, 573.
(10) Amundson, K. R.; Kalika, D. S.; Shen, M.; Yu, X.; Denn, M. M.; Reimer, J. A. *Mol. Cryst. Liq. Cryst.* **1987**, *153*, 271.
(11) Clements, J.; Humphreys, J.; Ward, I. M. *J. Polym. Sci., Polym. Phys. Ed.* **1986**, *24*, 2293.
(12) Mitchell, G. R.; Ishii, F. *Polym. Commun.* **1985**, *26*, 34.
(13) Jackson, W. J.; Kuhfuss, H. F. *J. Polym. Sci., Polym. Chem. Ed.* **1976**, *14*, 2043.
(14) Kalika, D. S.; Giles, D. W.; Denn, M. M. *J. Rheol.* **1990**, *34*, 139.
(15) Amundson, K. R. Ph.D. Thesis, University of California, 1989.
(16) Sefcik, M. D.; Schaefer, J.; Stejskal, E. O.; McKay, R. A. *Macromolecules* **1980**, *13*, 1132.
(17) McBrierty, V. J.; Douglass, D. C. *Phys. Rep.* **1980**, *63*, 61.
(18) Hentschel, R.; Schlitter, J.; Sillescu, H.; Spiess, H. W. *J. Chem. Phys.* **1978**, *68*, 56.
(19) Wolf, D. *Spin-Temperature and Nuclear-Spin Relaxation in Matter; Basic Principles and Applications*; Oxford University Press (Clarendon): Oxford, 1979; Chapter 10.
(20) Doane, J. W. In *Magnetic Resonance of Phase Transitions*; Owens, F. J., Poole, C. P., Jr., Farach, H. A., Eds.; Academic Press: New York, 1979; Chapter 4.
(21) In the weak-collision limit, the spin–lattice relaxation rate should be proportional to the correlation time times a prefactor, which is the square of the amplitude of dipolar fluctuations. Given the nature of the cooperative motion involved in relaxation, it is expected that the prefactor increases roughly proportional to the thermal energy. Multiplication of the abscissa by the inverse temperature compensates for this increase. This correction has only a slight effect on the calculation of the activation energy.
(22) Abragam, A. *Principles of Nuclear Magnetism*; Clarendon Press: New York, 1961.
(23) Murphy, P. D.; Taki, T.; Gerstein, B. C.; Henrichs, P. M.; Massa, D. J. *J. Magn. Reson.* **1982**, *49*, 99.
(24) VanderHart, D. L.; Böhm, G. C. A.; Mochel, V. D. *Polym. Prepr. (Am. Chem. Soc., Div. Polym. Chem.)* **1981**, *22* (2), 261.
(25) Fyfe, C. A.; Lyerla, J. R.; Bolksen, W.; Yannoni, C. S. *Macromolecules* **1979**, *12*, 757.
(26) Havens, J. R.; VanderHart, D. L. *Macromolecules* **1985**, *18*, 1663.
(27) Lowe, I. J.; Gade, S. *Phys. Rev.* **1967**, *156*, 817.
(28) Menczel, J.; Wunderlich, B. *J. Polymer Sci., Polym. Phys. Ed.* **1980**, *18*, 1433.
(29) Using physical and computer models of random HBA and ETP monomer sequences, the aromatic ring substitution axes were found to be typically aligned to within seven degrees of the local chain axis.
(30) English, A. D. *Macromolecules* **1984**, *17*, 2182.
(31) Schaefer, J.; Stejskal, E. O.; Steger, T. R.; Sefcik, M. D.; McKay, R. A. *Macromolecules* **1980**, *13*, 1121.
(32) Windle, A. H.; Viney, C.; Golombok, R.; Donald, A. M.; Mitchell, G. R. *Faraday Discuss., Chem. Soc.* **1985**, *79*, 55.

Registry No. (HBA)(ETP) (copolymer), 25822-54-2.